

## Detailed-term-accounting-approximation simulation of x-ray transmission through laser-produced Al plasmas

Jiaolong Zeng, Fengtao Jin, Jianmin Yuan, and Qisheng Lu

*Department of Applied Physics, National University of Defense Technology, Changsha 410073, People's Republic of China*

Yongsheng Sun

*Institute of Applied Physics and Computational Mathematics, Beijing 100088, People's Republic of China*

(Received 13 April 2000; revised manuscript received 14 July 2000)

An extensive configuration interaction (CI) scheme and the  $R$ -matrix method are combined to calculate the x-ray transmission spectrum for high-power laser-produced Al plasmas in local thermodynamic equilibrium by using the detailed-term-accounting (DTA) approximation. All atomic parameters such as state levels and photoabsorption cross sections for different ionization stages are obtained by using the CI and  $R$ -matrix method. Special attention is given to the effects of autoionizing resonance broadening on the transmission. A large difference exists between the convergence of the results with and without taking account of autoionizing resonance broadening when the autoionization resonance broadening is the major broadening mechanism. This shows that autoionizing resonance widths of the  $K$ -shell excited states have large effects and should be considered to interpret the spectral-resolved transmission.

PACS number(s): 52.25.Nr, 52.20.-j, 32.80.Hd

### I. INTRODUCTION

The absorption spectra of high-temperature plasmas have been of great utility in the study of inertial confinement fusion, x-ray lasers, opacity calculation, and magnetic fusion energy plasmas. In the past two decades, Al plasma had been of particular interest. Many experimental [1–4] and theoretical researches [5–10] considered the x-ray transmission spectrum of laser-produced Al plasmas. Davidson *et al.* [1,2] measured the transmission of x rays from external sources of known intensity through an aluminum plasma that was created by indirect laser irradiation. Local thermodynamic equilibrium (LTE) was obtained in their experiment and its x-ray absorption properties were measured. The experiments yield a plasma of about 40 eV temperature and 0.005 of solid density with the aluminum ions having 4–8 bound electrons. The measured transmission spectrum is in the photon energy range of 1480–1580 eV, corresponding to the inner-shell excitations from the  $1s$  electron to  $2p$  orbital. Perry *et al.* [3] made a similar experiment, but the experimental condition was slightly modified. Al XII through Al VIII had been made in a laser-heated slab plasma at the measured temperature and density of  $58 \pm 4$  eV and  $0.020 \pm 0.007$  g/cm<sup>3</sup>. Perry *et al.* [4] also made a radiation transfer experiment by using the  $K$ -shell absorption spectra and Iglesias *et al.* [10] did a detailed analysis of the experiment. Besides the direct opacity measurements of the Al plasma, a lot of experiments (see, for example, [11,12]) had used the x-ray transmission spectrum of Al as the temperature and density diagnostics.

Theoretical modeling for the absorption spectra of laser-produced plasma requires a great number of atomic data, state populations, spectral line shapes, and plasma conditions. As for the spectral line shapes, there are several broadening mechanisms, such as the natural width, autoionizing resonance, and collision and Doppler broadening. In principle, all these broadening mechanisms should be considered in a complete treatment, while in practice only the main fac-

tors are considered. A few theoretical calculations [5–9] on the transmission of Al plasmas have been carried out since the publication of the experiments of Davidson *et al.* [1,2]. But most of them had only taken account of Doppler broadening in calculating the line absorption cross section. Kilcrease *et al.* [5] and Rose [6] carried out atomic configuration average simulations for the experimental plasma spectroscopy with Gaussian profile whose widths were calculated from the unresolved transition array (UTA) approximation [13]. Abdallah and Clark [7] did a detailed calculation by including the fine structure. All these calculations treated approximately the  $K$ -shell excited states as discrete ones and used the Gaussian profile for the spectral line shape with Doppler width. A configuration interaction (CI) calculation was carried out by Iglesias *et al.* [8] with orbital wave functions computed using the Dirac-Hatree-Slater (DHS) method. They used a Voigt profile including electron collision broadening and Doppler widths. Actually, these  $K$ -shell excited states are well above the ionization threshold and the photoexcitations of a  $1s$  electron to the  $2p$  orbital are autoionization processes. As will be demonstrated later, the autoionizing resonance widths play an important role in determining the photoabsorption cross sections and, hence, transmission spectrum.

The purpose of the present work is to calculate the x-ray transmission spectrum of the Al plasma with the prototype experimental conditions of Davidson *et al.* [1,2] and Perry *et al.* [3]. The transitions of one electron excited from the  $1s$  electron to  $2p$  orbital are treated as autoionization processes by using the close-coupling scheme with special attention given to the effects of autoionizing resonance widths on the transmission. The calculations have considered photoexcitation and photoionization processes. Free-free absorption and scattering are assumed to be negligible for the present work. All relevant atomic physics data are calculated by using the atomic structure codes CIV3 [14] and MCHF [15] and the latest  $R$ -matrix code [16].

## II. METHOD OF CALCULATION

For an LTE plasma, the population distributions of different ionization stages are given by the Saha equation [17]

$$\frac{N_{i+1}N_e}{N_i} = \frac{Z_e Z_{i+1}}{Z_i} e^{-(\phi_i - \Delta\phi_i)/kT}, \quad (1)$$

where  $N_i$  is the total population density of ion  $i$ ,  $N_e$  is the number of free electrons per unit volume,  $\phi_i$  is the ionization potential of ion  $i$ ,  $\Delta\phi_i$  is the depression of ionization limit caused by the plasma environment restricting the number of bound states available, and  $Z_i$  and  $Z_e$  are the partition functions for ion  $i$  and the free electron, respectively.  $Z_i$  is given by

$$Z_i = \sum_t g_{it} e^{-E_{it}/kT} \quad (2)$$

and  $Z_e$  by

$$Z_e = 2 \left( \frac{2\pi m_e kT}{h^2} \right)^{3/2}, \quad (3)$$

where  $g_{it} = (2L_{it} + 1)(2S_{it} + 1)$  is the statistical weight for term  $t$  of ion  $i$  in the  $LS$  coupling condition,  $L_{it}$  and  $S_{it}$  are the total angular momentum and spin quantum numbers, respectively,  $E_{it}$  is the energy of term  $t$  of ion  $i$  above the ground state,  $k$  is the Boltzmann constant,  $T$  is the temperature,  $m_e$  is the electron mass, and  $h$  is the Planck constant. The upper limit to the sum (2) is given by the same ionization depression as for the Saha equation. The population density  $N_{it}$  for term  $t$  of ion stage  $i$  is given by the Boltzmann distribution function

$$N_{it} = g_{it} (N_i / Z_i) e^{-E_{it}/kT}. \quad (4)$$

Equation (1) is solved with the constraint of particle and charge conservation.

In solving the Saha equation (1), a calculation of the ionization potential depression (IPD) is needed to give a finite limit to the partition functions. There are a number of methods by which the IPD can be calculated (for example, see [18]), such as the Debye-Huckel model, Stewart-Pyatt approximation, and the ion-sphere model. It is well known that the use of the IPD in this manner leads to discontinuous derivatives of the free energy, but it is not important for interpreting experimental results. As the influence on the transmission spectrum due to the three different models is small, we choose the first one. For the Debye-Huckel model of the plasma potential, the largest radius of an electron that can still be bound is given by the Debye radius. As the principal quantum number becomes larger, the ions behave more and more hydrogenically. In this case the IPD is given by

$$\Delta\phi_i = \frac{ze^2}{4\pi\epsilon_0} \sqrt{\frac{e^2 N_e}{\epsilon_0 kT}}, \quad (5)$$

where  $z$  is the charge of the species of interest ( $z=1$  for neutral). The calculated IPD's for different relevant ionization stages under the experimental conditions of Davidson *et al.* [1,2] and Perry *et al.* [3] using the Debye model are

TABLE I. Calculated IPD (in Ry) under the experimental conditions of Davidson *et al.* and Perry *et al.* [3].

Davidson <i>et al.</i>	IPD	Perry <i>et al.</i>	IPD
Al v	0.5114	Al vii	0.8012
Al vi	0.6137	Al viii	0.9229
Al vii	0.7160	Al ix	1.0382
Al viii	0.8183	Al x	1.1536
Al ix	0.9206	Al xi	1.2689
Al x	1.0229	Al xii	1.3843

listed in Table I. The maximum effective principal quantum number is nearly equal to 7 for the former experiment and 8 for the latter. This is consistent with the calculation carried out by Iglesias *et al.* [8] with a limit of  $n \leq 7$  in simulating the former experiment. From the calculated IPD and the maximum effective principal quantum number  $n=8$ , we include, as did by Iglesias *et al.* [10], the states from the following configurations for each ionization stage:

$$1s^2 2l^m, \quad 1s^2 2l^{m-1} n'l',$$

as well as

$$1s 2l^{m+1}, \quad 1s 2l^m n'l',$$

for all  $3 \leq n' \leq 8$  and  $l' \leq 4$  ( $g$  orbitals). The sum (2) is limited to the above available bound terms which takes account of the IPD. The calculated partition functions (2) and IPDs are used to solve the Saha equation (1).

The absorption coefficient for radiation of energy  $h\nu$  for a plasma of particle density  $N$  and temperature  $T$  is given by

$$\mu(h\nu) = \sum_i N_i \sigma_i(h\nu), \quad (6)$$

where  $\sigma_i(h\nu)$  is the photoabsorption cross section per ion  $i$  and  $h\nu$  is the photon energy. It can be calculated from the photoabsorption cross section  $\sigma_{it}(h\nu)$  from term  $t$  in ion  $i$ :

$$\sigma_i(h\nu) = \sum_t \frac{g_{it} e^{-E_{it}/kT}}{Z_i} \sigma_{it}(h\nu). \quad (7)$$

The photoabsorption (including photoexcitation and photoionization) cross section  $\sigma_{it}(h\nu)$  is calculated by the  $R$ -matrix code [16] in a consistent way. We should treat the inner-shell photoexcitation processes as autoionizing ones because the final states of the transitions are well above the ionization threshold and they are actually autoionizing states. The calculated photoabsorption cross sections are convolved with Doppler broadening. In this way, both the autoionization resonance width and Doppler broadening can be considered. The sum in Eq. (7) is carried out over all available bound states.

The  $R$ -matrix method for electron-atom and photon-atom interactions has been discussed in great detail by Burke *et al.* [19]. In an  $R$ -matrix calculation, the wave function of the  $(N+1)$ -electron system is given the form

$$\begin{aligned}
\Psi_k(X_1, \dots, X_{N+1}) \\
= \hat{A} \sum_{ij} c_{ijk} \Phi_i(X_1, \dots, X_N, \hat{\mathbf{r}}_{N+1}, \sigma_{N+1}) \times u_{ij}(r_{N+1}) \\
+ \sum_j d_{jk} \phi_j(X_1, \dots, X_{N+1}), \quad (8)
\end{aligned}$$

where  $\hat{A}$  is the antisymmetrization operator to take the exchange effect between the target electrons and the free electron into account.  $X_i$  stands for the spatial ( $\mathbf{r}_i$ ) and the spin ( $\sigma_i$ ) coordinates of the  $i$ th electron. The functions  $u_{ij}(r)$  under the first sum construct the basis sets for the continuum wave functions of the free electron, and  $\Phi_i$  are the coupling between the target states and the angular and spin part of the free electron. The correlation functions  $\phi_j$  in the second sum are constructed by the square integrable orbitals to account for correlation effects not adequately considered because of the cutoff in the first sum. Although general atomic codes such as CIV3 [14] and MCDF [20] or other relativistic parametric potential codes [21] can account for extensive CI, a close-coupling scheme such as the  $R$ -matrix method can account for correlation effects between the free and bound electrons and the couplings between different channels. Thus the  $R$ -matrix method can give more accurate atomic data such as the energy levels and densities of the oscillator strength of the inner-shell excited autoionizing states. More importantly, the autoionizing resonance widths are naturally included in the  $R$ -matrix calculation. The effectiveness of the  $R$ -matrix method had been demonstrated clearly by some most recent calculations [22–25]. Voky *et al.* [22,23] carried out inner-shell photoionization calculations of ground-state lithium in the photon energy regions below 130 eV including  $1snln'l'$  Rydberg resonance series and of hollow atomic states by using the  $R$ -matrix method. Zhou *et al.* [24] have calculated the inner-shell photoionization of  $1s^22p^2P^o$  and  $1s^23p^2P^o$  excited states of Li by using the same  $R$ -matrix method. The wave functions of the target states in all these calculations have been determined by using the code CIV3 [14]. Their calculated resonance energy positions  $1snln'l'$  and  $2l2l'n''l''$  are in good agreement with experiment. We [25] have also calculated the inner-shell photoionization of the ground and the first excited states of lithiumlike carbon and also obtained excellent agreement between the theoretical and experimental energy levels of the inner-shell excited autoionizing states of CIV ions.

The fraction of radiation transmitted,  $F$ , at energy  $h\nu$  with respect to some incident source of arbitrary intensity is given by

$$F(h\nu) = e^{-\mu(h\nu)L}, \quad (9)$$

where  $L$  is the path length traversed by the light source through the plasma. The function  $F$  is integrated over a Gaussian function, with the full width at half maximum (FWHM) corresponding to the spectrometer resolution, to obtain the final transmission spectrum. Because the transmission  $F(h\nu)$  is not a linear function of the absorption coefficient  $\mu(h\nu)$ , the averaged  $F(h\nu)$  over the experimental resolution depends on the spectral linewidths in  $\mu(h\nu)$ .

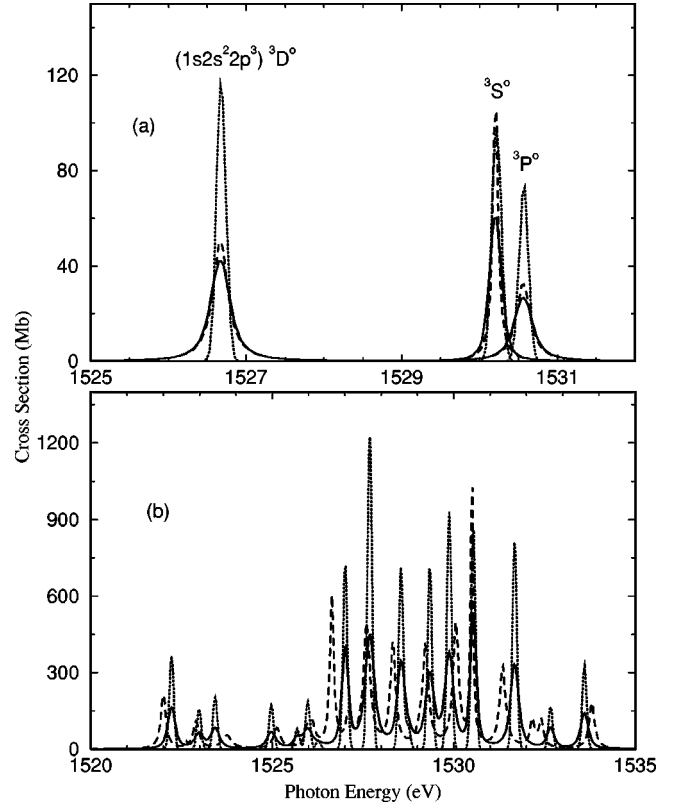


FIG. 1. Comparisons of the effects of three line shapes, Voigt, Lorentzian, and Gaussian, on the photoabsorption cross sections. (a) From the ground state of  $\text{Al}^{7+}$  and (b) the sum of the first 12 low-lying states with the consideration of statistical weights and relative energies to the ground state. Solid, dashed, and dotted lines refer to Voigt, Lorentzian, and Gaussian profiles, respectively.

### III. RESULTS AND DISCUSSION

First, we check the influence of the autoionizing widths on the convergence behavior of our calculation by simulating the prototype experiment done by Davidson *et al.* The FWHM of Doppler broadening is approximately 0.14 eV for an aluminum plasma at  $kT=40$  eV and a photon energy of 1500 eV. The effect of electron collision broadening was estimated [26] to be a factor of 5 less than the Doppler width for the plasma conditions and the photon energy range of interest. But the autoionizing resonance width may be larger than the Doppler width and becomes the major broadening mechanism. To have a quantitative understanding of the autoionizing resonance widths, we take  $\text{Al}^{7+}$  as an example. Figure 1(a) shows the photoabsorption cross sections near the  $K$ -shell resonances with three different line profiles for the ground state  $2s^22p^2\ ^3P^o$  of  $\text{Al}^{7+}$ . The three resonances are caused by three  $1s2s^22p^3\ ^3S^o$ ,  $^3P^o$ ,  $^3D^o$  autoionizing states. The solid line refers to the Voigt profile which is obtained by convolving the  $R$ -matrix result with Doppler broadening, the dashed line to the  $R$ -matrix result which assumes Lorentzian profile, and the dotted line to the Gaussian profile which includes the Doppler broadening alone. The dotted line is obtained by treating the transitions as bound-bound processes and using the oscillator strengths calculated by the CIV3 atomic structure code [14]. The corresponding cross section for a given line can be expressed in terms of the oscillator strength  $f_{iiv'}$  as

$$\sigma_{it'} = \frac{\pi h e^2}{m_e c} f_{it'} S(h\nu) = 109.71 f_{it'} S(h\nu), \quad (10)$$

where  $S$  is the line shape function with  $h\nu$  in eV and  $\sigma_{it'}$  in Mb. If only the Doppler broadening is considered, the line shape function  $S$  has a Gaussian profile

$$S(h\nu) = \frac{\sqrt{\ln 2}}{\sqrt{\pi} \Gamma} e^{-\ln 2 (h\nu - h\nu_0)^2 / \Gamma^2}, \quad (11)$$

where  $h\nu_0$  is the transition energy, and  $2\Gamma$  is the FWHM and taken as the Doppler width.

In general, the observed spectral profile is neither simply Gaussian nor Lorentzian, but a convolution of these two profiles,

$$S(h\nu) = \frac{\sqrt{\ln 2}}{\pi \Gamma} H(a, \nu), \quad (12)$$

where  $H(a, \nu)$  is the Voigt function:

$$H(a, \nu) = \frac{a}{\pi} \int_{-\infty}^{+\infty} \frac{\exp(-x^2)}{a^2 + (\nu - x)^2} dx,$$

$$a = \sqrt{\ln 2} \Gamma_l / \Gamma,$$

$$\nu = \sqrt{\ln 2} (h\nu - h\nu_0) / \Gamma,$$

$$\Gamma = \Gamma_l + \Gamma_d,$$

where  $h\nu$  is the photon energy,  $\Gamma_l$  is the Lorentzian FWHM due to the resonance and collision broadening mechanisms, and  $\Gamma_d$  is the Doppler FWHM.

In performing the  $R$ -matrix calculation which allows for  $1s$  being excited to the  $2p$  subshell, we include six orbitals  $1s, 2s, 2p, 3s, 3p,$  and  $3d$ . Fourteen  $\text{Al}^{8+}$  target states are included in the close-coupling wave function expansion:  $1s^2 2s^2 2p^2 ({}^2P^o), 1s^2 2s 2p^2 ({}^4P^e, {}^2D^e, {}^2S^e, {}^2P^e), 1s^2 2p^3 ({}^4S^o, {}^2D^o, {}^2P^o), 1s^2 2s^2 3s ({}^2S^e), 1s^2 2s^2 3p ({}^2P^o),$  and  $1s 2s^2 2p^2 ({}^4P^e, {}^2D^e, {}^2S^e, {}^2P^e)$ . The calculated ionization potential is 20.9110 Ry, differing from the experimental value of 20.9176 Ry by only 0.031%. Autoionizing resonance widths can be obtained by analyzing the resonance structures of our  $R$ -matrix result. They are 0.24, 0.09, and 0.22 eV, respectively, for the three  $1s 2s^2 2p^3 {}^3S^o, {}^3P^o,$  and  ${}^3D^o$  autoionizing states. Two of them (0.24 and 0.22 eV) are larger than the Doppler widths of approximately 0.14 eV. The transition energies obtained by CIV3 are shifted a little in order to have a direct comparison with the  $R$ -matrix calculation. One can easily see that the Voigt and Lorentzian profiles differ considerably from the Gaussian profile, and thus can give different contributions to the transmission.

In addition to the ground state, the other 11 lowest states ( $2s^2 2p^2 {}^1D, {}^1S, 2s 2p^3 {}^5S^o, {}^3D^o, {}^3P^o, {}^1D^o, {}^3S^o, {}^1P^o,$  and  $2p^4 {}^3P, {}^1D, {}^1S$ ) have relatively large contributions to the photoabsorption cross sections because of their relatively low energies relative to the ground state. There are 24 inner-shell transitions in total related to these low-lying states (including the ground state). The sum of their contributions to the photoabsorption cross sections is shown in Fig. 1(b) with

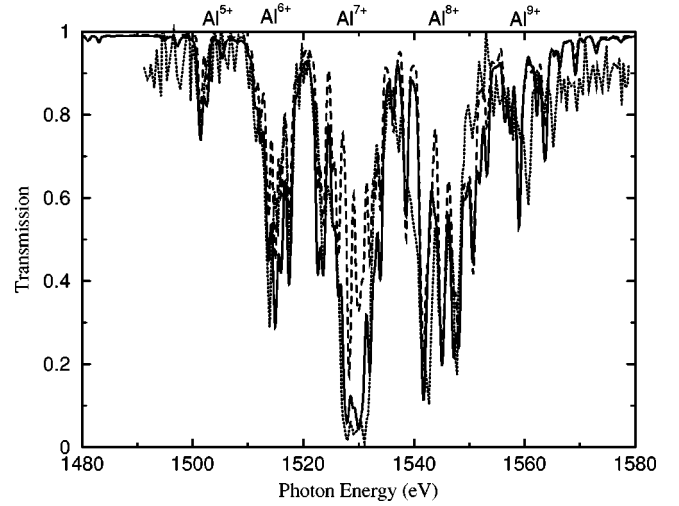


FIG. 2. Transmission calculated as a function of photon energy in eV by using the CIV3 code with instrumental broadening has been considered. The temperature and density are 40 eV and 0.0135 g/cm<sup>3</sup>, respectively. The solid and dashed lines refer to the theoretical results with Voigt and Gaussian line shape functions, respectively. The dotted line refers to the experimental spectrum. The labels at the top of the figure indicate the dominant ion charge states of aluminum in each energy region.

the consideration of statistical weights and relative energies to the ground state. The meaning of the lines is the same as plot 1(a). The position of lines calculated by CIV3 has been shifted toward a lower photon energy by 0.34 eV to fit the  $R$ -matrix result. The result by the  $R$ -matrix method should be more reliable because the  $R$ -matrix method can give accurate energies of inner-shell excited states [25]. One can see clearly that there are windows between the spectral lines of the Gaussian profile when the autoionizing effect is ignored completely. These windows can be narrowed by the spin split of the spectral lines due to relativistic effects, but cannot be blocked sufficiently. These windows are the main cause of the difference in the calculated x-ray transmission shown later in Fig. 2. In contrast, Lorentzian and Voigt profiles have considerable line blending to smear the windows effectively.

The effect of autoionizing resonance broadening on the transmission can be seen more clearly from Fig. 2, where the calculated transmission has been convolved with the spectrometer resolution 0.7 eV, which is the same as that used by Abdallah and Clark [7]. To simulate the experiment, the path length  $L$  is chosen to be 0.004 cm. The results presented in Fig. 2 are not obtained by the  $R$ -matrix calculation. The optical transitions are treated as bound-bound processes as described by Eq. (10), but two line profiles, Voigt and Gaussian, are used in the calculations. The width of the Voigt profile was determined by a convolution of a Lorentzian profile and a Gaussian profile as described by Eq. (12). The width of the Lorentzian profile is taken approximately to be the autoionizing width, which is obtained by the corresponding  $R$ -matrix calculation, and the width of the Gaussian profile is taken to be the Doppler width. For these results, the absorption coefficient for radiation of energy  $h\nu$  is given by

$$\mu(h\nu) = \sum_i \left( \sum_{it'} N_{it} \sigma_{it'}(h\nu) + \sum_t N_{it} \sigma'_{it}(h\nu) \right), \quad (13)$$

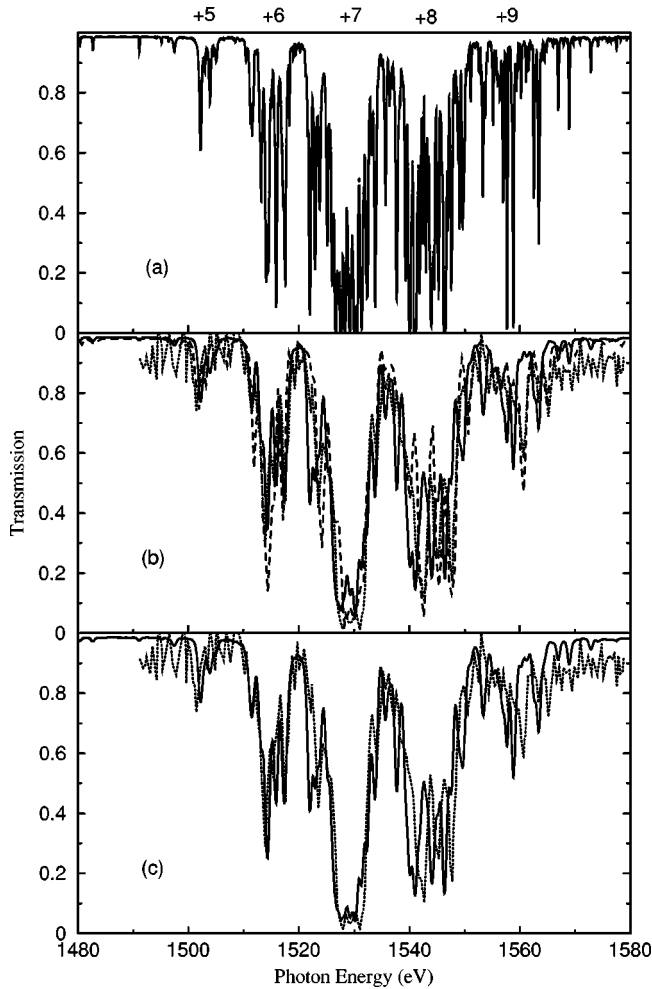


FIG. 3. Transmission calculated as a function of photon energy in eV by using the  $R$ -matrix method. The temperature and density are 40 eV and  $0.0135 \text{ g/cm}^3$ , respectively. In (a), the solid and dashed lines refer to the length and velocity forms by using the Voigt profile. The agreement between the two forms is so good that they cannot be distinguished. In (b), the solid line is obtained by integrating curve (a) using the reported spectrometer resolution, and the dashed one is the result of Abdallah and Clark [7]. In (c), the solid line refers to the result obtained by combining the  $R$ -matrix and CIV3 CI methods to include more satellite lines. In (b) and (c), the dotted line refers to the experimental spectrum carried out by Davidson *et al.*

where  $\sigma_{it'}(h\nu)$  is the cross section for the bound-bound transition from term  $t$  to  $t'$ , and  $\sigma_{it}^i(h\nu)$  is the total photoionization cross section from term  $t$  without the autoionizing resonances. The solid line refers to the final transmission spectrum obtained by using the Voigt profile, the dashed one to the transmission spectrum by Gaussian profile, and the dotted one to the experimentally observed spectrum. The labels at the top of the figure indicate the dominant  $i$  charge states of aluminum in each energy region. As our  $R$ -matrix calculation, which will be shown in Fig. 3 later, includes approximately all terms up to  $n=5$ , we include all orbitals up to  $n=5$  in the result shown in Fig. 2. The agreement between the calculated spectrum using the Voigt profile and the experimental spectrum is good for both the spectral intensity and position, but a large difference exists by using the Gaussian profile, especially for the lower ionization stages

such as  $\text{Al}^{5+}$ ,  $\text{Al}^{6+}$ , and  $\text{Al}^{7+}$ . This is because these ions have relatively large autoionizing resonance widths. According to the  $R$ -matrix calculation, the typical autoionizing resonance widths are approximately 0.29, 0.24, 0.20, 0.11, and 0.08 eV from  $\text{Al}^{5+}$  to  $\text{Al}^{9+}$ , respectively. From the comparison of the two calculated spectra with the experimental result, one can conclude that the theoretical calculations with only taking account of the Doppler broadening would result in a too slower convergence to the observed spectra. For the  $K$ -shell transitions from the low-lying states, autoionizing resonance broadening, an actually existing physical effect, is the major broadening mechanism and should be taken into account in calculating the spectral-resolved transmission.

The transmission spectrum obtained by using the  $R$ -matrix photoabsorption cross sections is given in Fig. 3. In order to demonstrate the convergence of the result with the model size of the calculation, we take  $\text{Al}^{7+}$  as an example. In addition to the main transitions from the low-lying states, the satellite transitions from the highly excited states have been included in our consideration by the  $R$ -matrix method allowing for  $1s$ - $2p$  resonances. In total, photoabsorption cross sections of 129 terms are included in the calculations of the absorption coefficient of  $\text{Al}^{7+}$  ions. For each term, we have so many autoionization resonances that are approximately equivalent to 500–1500 discrete relativistic transitions, and in total we have more than 100 000 transitions for the  $\text{Al}^{7+}$  ions, which is one order less than the numbers of oscillator strengths considered by Abdallah and Clark [7]. The highest one of the 129 terms for the  $\text{Al}^{7+}$  ions is 18.4 Ry above the ground state. All the data of other relevant ionization stages are obtained by similar method. They are convolved with Doppler widths and combined to obtain the transmission which is shown in Fig. 3. Figure 3(a) shows the transmission which has not included instrumental broadening. This spectrum is highly resolved and shows that many  $1s$ - $2p$  lines are contributing to the transmission. Figure 3(b) shows a solid line derived by convolving the curve shown in Fig. 3(a) with spectrometer resolution. The dotted line shows the experimental spectrum. The calculated spectrum is in satisfactorily good agreement with the experiment. Not only are all the major structures present, but also the intensities agree well. Except for  $\text{Al}^{7+}$ , the positions of the spectrum of other ionization stages have a small shift compared to the experimental spectrum.  $\text{Al}^{8+}$  and  $\text{Al}^{9+}$  shift toward a lower photon energy, while  $\text{Al}^{5+}$  and  $\text{Al}^{6+}$  shift a little toward a higher photon energy. This may be due to the fact that different ions have different electrons and thus different correlation energies. For comparison, we also give the theoretical spectrum of Abdallah and Clark [7] with a dashed line. They obtained the results by carrying out a much larger size calculation than ours. In their treatment, oscillator strengths were computed for all possible bound-bound transitions among all possible excited electron orbitals with  $n < 11$  and  $l < 5$ . Good agreement was also obtained by Iglesias *et al.* [8] with a limit of  $n < 8$  and  $l < n$ . What we can conclude is that their calculations converge with electron orbitals slower than the present case due to the neglect of the autoionization resonance broadening.

In order to make the  $R$ -matrix calculations manageable, we only include orbitals up to  $n=3$ . The contributions of some satellite lines from highly excited states are not in-

cluded in the calculations. In order to access the convergence of the present  $R$ -matrix calculation, we have included more satellite lines by using the CIV3 code. In this calculation, in addition to the transitions treated by the  $R$ -matrix scheme, we have considered more satellite lines with the initial states above the highest term treated by the  $R$ -matrix method. These additional satellite lines are restricted to the excited states of having one electron in the orbitals of  $3 \leq n' \leq 8$  and  $l' \leq 4$ . Because the autoionizing width of these satellite lines are much smaller than the Doppler width, their inclusion by using the CIV3 code does not reduce the generality of this method. The result is shown in Fig. 3(c). It can be easily seen that our  $R$ -matrix calculation is basically converged. The inclusion of the contributions of more satellite lines can improve the final spectrum slightly.

Now, let us turn to the experiment done by Perry *et al.* [3]. In this experiment, the main ionization stages ranged from Al VIII to Al XII and the typical Doppler FWHM of  $1s$  to  $2p$  transitions is approximately 0.18 eV. Because of different experimental conditions, higher ionization stages had been created than in the experiment by Davidson *et al.* As has been shown above, the autoionizing resonance widths of the  $K$ -shell excited states of the ions present in the experiment of Perry *et al.* [3] are less than Doppler broadening and Doppler broadening becomes the main broadening mechanism. For this case, the inclusion of autoionizing resonance broadening will not change the convergence behavior as much as in the above calculation, and the relativistic effect may have a large influence on the transmission spectrum. Figure 4 shows the results obtained by multiconfiguration Hartree-Fock (MCHF) [15] calculations with both the  $LS$  nonrelativistic and the Breit-Pauli  $LSJ$  relativistic formalisms. The solid line refers to the relativistic calculation and the dashed one to the nonrelativistic result. The dotted line refers to the experimental spectrum. In performing the MCHF calculation, the maximum principal and angular momentum quantum numbers of the orbitals are considered up to  $n' = 8$  and  $l' = 5$  ( $h$  orbitals). In order to directly compare the experimental spectrum, the calculated spectrum was shifted to lower photon energy by about 3.0 eV. One can easily see that rather good agreement is obtained between the calculated and experimental spectra after taking account of the relativistic splitting.

In conclusion, the x-ray transmission spectrum is calculated for an Al plasma by using the detailed-term-accounting (DTA) model. The  $R$ -matrix method is applied to simulate

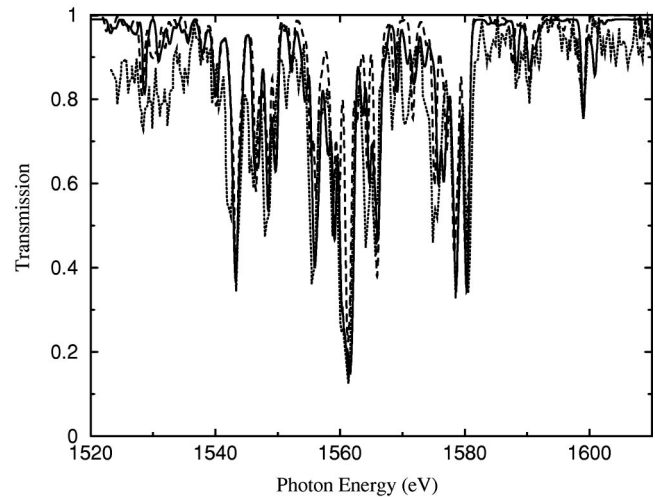


FIG. 4. Transmission calculated as a function of photon energy in eV under the experimental condition of Perry *et al.* [3] with temperature  $T = 58$  eV and density  $\rho = 0.02$  g/cm<sup>3</sup> by using MCHF  $LS$  nonrelativistic (dashed line) and  $LSJ$  relativistic formalisms (solid line) compared with the experiment (dotted line).

the x-ray transmission spectrum. The importance of the autoionizing widths of the spectral lines of  $1s$ - $2p$  transitions to the convergence of the result with the model size is demonstrated by two ways. The first one treats the  $1s$ - $2p$  transitions approximately as bound-bound processes and takes the autoionizing effect into account by using the Voigt profile. The second one considers the autoionizing effect more naturally by using a close-coupling scheme. Both calculations arrive at good agreement with the experiment and prove that fewer electron orbitals are required to obtain a converged result in the case that  $1s$ - $2p$  autoionizing resonance broadening is the major broadening mechanism. For higher ionization stages, such as Al X and Al XI, the autoionizing resonance widths are less than the Doppler widths and the convergence of the theory is determined by Doppler broadening and the relativistic effect.

#### ACKNOWLEDGMENTS

This work was supported by the National Natural Science Foundation of China under Grant No. 19974075, the Science Foundation of China Academy of Engineering Physics under Grant No. 95009, and the China Research Association of Atomic and Molecular Data.

- [1] S.J. Davidson, J.M. Foster, C.C. Smith, K.A. Warburton, and S.J. Rose, *Appl. Phys. Lett.* **52**, 847 (1988).
- [2] S.J. Davidson, C.L.S. Lewis, D. O'Neill, S.J. Rose, J.M. Foster, and C.C. Smith, in *Laser Interaction with Matter*, edited by G. Velarde, E. Minguez, and J.M. Perlado (World Scientific, Singapore, 1989).
- [3] T.S. Perry, S.J. Davidson, F.J.D. Serduke, D.R. Bach, C.C. Smith, J.M. Foster, R.J. Doyas, R.A. Ward, C.A. Iglesias, F.J. Rogers, J.Jr. Abdallah, R.E. Stewart, J.D. Kilkenny, and R.W. Lee, *Phys. Rev. Lett.* **67**, 3784 (1991).
- [4] T.S. Perry, R.A. Ward, D.R. Bach, R.J. Doyas, B.A. Hammel,

- D.W. Phillion, H.N. Kornblum, J.M. Foster, P.A. Rosen, R.J. Wallace, and J.D. Kilkenny, *J. Quant. Spectrosc. Radiat. Transf.* **51**, 273 (1994).
- [5] D.P. Kilcrease, J.Jr. Abdallah, J.J. Keady, and R.E.H. Clark, *J. Phys. B* **26**, L717 (1993).
- [6] S.J. Rose, *J. Phys. B* **25**, 1667 (1992).
- [7] J.Jr. Abdallah, and R.E.H. Clark, *J. Appl. Phys.* **69**, 23 (1991).
- [8] C.A. Iglesias, J.K. Nash, M.H. Chen, and F.J. Rogers, *J. Quant. Spectrosc. Radiat. Transf.* **51**, 125 (1994).
- [9] A. Rickert, *J. Quant. Spectrosc. Radiat. Transf.* **54**, 325 (1995); S.J. Rose, *ibid.* **51**, 317 (1994).

- [10] C.A. Iglesias, M.H. Chen, D.L. McWilliams, J.K. Nash, and F.J. Rogers, *J. Quant. Spectrosc. Radiat. Transf.* **54**, 185 (1995).
- [11] J.M. Foster, D.J. Hoarty, C.C. Smith, P.A. Rosen, S.J. Davidson, S.J. Rose, T.S. Perry, and F.J.D. Serduke, *Phys. Rev. Lett.* **67**, 3255 (1991).
- [12] T.S. Perry, P.T. Springer, D.F. Fields, D.R. Bach, F.J.D. Serduke, C.A. Iglesias, F.J. Rogers, J.K. Nash, M.H. Chen, B.G. Wilson, W.H. Goldstein, B. Rozsynai, R.A. Ward, J.D. Killenny, R. Doyas, L.B. Da Silva, C.A. Back, R. Cauble, S.J. Davidson, J.M. Foster, C.C. Smith, A. Bar-Shalom, and R.W. Lee, *Phys. Rev. E* **54**, 5617 (1996).
- [13] J. Bauche, C. Bauche-Arnoult, and M. Klapisch, *Adv. At. Mol. Phys.* **22**, 2503 (1987).
- [14] A. Hibbert, *Comput. Phys. Commun.* **9**, 141 (1975).
- [15] C.F. Fischer, *Comput. Phys. Commun.* **64**, 369 (1991).
- [16] K.A. Berrington, W.B. Essner, and P.H. Norrington, *Comput. Phys. Commun.* **92**, 290 (1995).
- [17] R.D. Cowan, *Theory of Atomic Spectra* (University of California Press, Berkeley, 1981).
- [18] D.J. Heading, J.S. Wark, G.R. Bennett, and R.W. Lee, *J. Quant. Spectrosc. Radiat. Transf.* **54**, 167 (1995), and references therein.
- [19] P.G. Burke, A. Hibbert, and W.D. Robb, *J. Phys. B* **4**, 153 (1971).
- [20] I.P. Grant, B.J. Mckenzie, P.H. Norrington, D.F. Mayers, and N.C. Pyper, *Comput. Phys. Commun.* **21**, 207 (1980).
- [21] F.J. Rogers, B.G. Wilson, and C.A. Iglesias, *Phys. Rev. A* **38**, 5007 (1988).
- [22] L. Voky, P. Faucher, A. Hibbert, J.-M. Li, Y.-Z. Qu, J. Yan, J.C. Chang, and F. Bely-Dubau, *Phys. Rev. A* **57**, 1045 (1998).
- [23] L. Voky, P. Faucher, H.L. Zhou, A. Hibbert, Y.-Z. Qu, J.-M. Li, and F. Bely-Dubau, *Phys. Rev. A* **58**, 3688 (1998).
- [24] H.L. Zhou, S.T. Manson, L. Voky, P. Faucher, F. Bely-Dubau, A. Hibbert, S. Diehl, D. Cubaynes, J.-M. Bizau, L. Journel, and F.W. Wuilleumier, *Phys. Rev. A* **59**, 462 (1999).
- [25] Jiaolong Zeng, Jianmin Yuan, Zengxiu Zhao, and Qisheng Lu, *Euro. Phys. J. D* (to be published).
- [26] B.H. Armstrong, R.R. Johnston, P.S. Kelly, H.E. Dewitt, and S.G. Brush, *Progress in High Temperature Physics and Chemistry* (Pergamon, Oxford, 1966), Vol. 1, p. 169.